Astron. Astrophys. 345, 681–690 (1999)

ASTRONOMY AND ASTROPHYSICS

ESO imaging survey

II. Searching for distant clusters of galaxies

L.F. Olsen[1,2], M. Scodeggio[1], L. da Costa[1], C. Benoist[1,3], E. Bertin[1,4,5], E. Deul[1,4], T. Erben[1,6], M.D. Guarnieri[1,7], R. Hook[8], M. Nonino[1,9], I. Prandoni[1,10], R. Slijkhuis[1,4], A. Wicenec[1], and R. Wichmann[1,11]

[1] European Southern Observatory, Karl-Schwarzschild-Strasse 2, D-85748 Garching bei München, Germany
[2] Astronomisk Observatorium, Juliane Maries Vej 30, DK-2100 Copenhagen, Denmark
[3] DAEC, Observatoire de Paris-Meudon, 5 Pl. J. Janssen, F-92195 Meudon Cedex, France
[4] Leiden Observatory, P.O. Box 9513, 2300 RA Leiden, The Netherlands
[5] Institut d'Astrophysique de Paris, 98bis Bd Arago, F-75014 Paris, France
[6] Max-Planck-Institut für Astrophysik, Postfach 1523, D-85748 Garching bei München, Germany
[7] Osservatorio Astronomico di Pino Torinese, Strada Osservatorio 20, I-10025 Torino, Italy
[8] Space Telescope – European Coordinating Facility, Karl-Schwarzschild-Strasse 2, D-85748 Garching bei München, Germany
[9] Osservatorio Astronomico di Trieste, Via G.B. Tiepolo 11, I-31144 Trieste, Italy
[10] Istituto di Radioastronomia del CNR, Via Gobetti 101, I-40129 Bologna, Italy
[11] Landensternwarte Heidelberg-Königstuhl, D-69117 Heidelberg, Germany

Received 1 April 1998 / Accepted 21 December 1999

Abstract. This paper presents preliminary results of a search for distant clusters of galaxies using the recently released I-band data obtained by the ESO Imaging Survey (EIS), covering about 3 square degrees. A matched filter algorithm is applied to the galaxy catalogs extracted from the two sets of frames that contiguously cover the whole surveyed area. From these catalogs two independent lists of cluster candidates are generated and used to establish, directly from the data, a robust detection threshold. In preparing the list of candidate clusters the main concern has been to avoid the inclusion of spurious detections. A preliminary catalog of 35 distant cluster candidates is presented, with estimated redshifts $0.2 \leq z \leq 1.0$ over an area of 2.5 square degrees, after excluding regions where the quality of the available data is poor.

Key words: galaxies: clusters: general – cosmology: observations – cosmology: large-scale structure of Universe

1. Introduction

One of the primary goals for undertaking the ESO Imaging Survey (EIS; Renzini & da Costa 1997) has been the preparation of a sample of optically-selected clusters of galaxies over an extended redshift baseline for follow-up observations with the VLT. High-redshift clusters are, of course, a primary target for 8-m class telescopes. A large sample of clusters can be used for many different studies, ranging from the evolution of the galaxy population, to the search for arcs and lensed high redshift galaxies, to the evolution of the abundance of galaxy clusters, a powerful discriminant of cosmological models. In addition, individual clusters may be used for weak lensing studies and as natural candidates for follow-up observations at X-ray and mm wavelengths, which would provide complementary information about the mass of the systems. For most of these applications it suffices to find a large number of clusters, while for others it is vital to have a full understanding of the selection effects, to generate suitable statistical samples.

The main goal of the present paper is to *timely* provide the astronomical community with a list of cluster candidates that can be used as individual targets for follow-up observations in the Southern Hemisphere, especially at the VLT. It must be emphasized that it is not the intention of the present paper to provide a complete and well-defined sample for statistical studies, since such analysis is beyond the scope of the present effort. This would require the derivation of the selection function characterizing the present sample (e.g., search algorithm parameters, observing conditions) and the comparison with the results from detections at different wavelengths (e.g., IR, X-ray).

Observations of the first patch of the EIS, covering about 3 square degrees, have been completed, and in March 1998 the data were made available to the community (Nonino et al. 1999; hereafter Paper I). In this paper object catalogs extracted from single 150 sec I-band images are used to identify cluster candidates using the matched filter method proposed by Postman et al. (1996, hereafter P96) and applied by these authors to analyze similar data. This method was chosen to allow a direct comparison with their results. However, since the data are publicly available, other groups may wish to produce their own catalogs

Send offprint requests to: L.F. Olsen

using other methods and choosing smaller but more uniform regions within the surveyed area. Comparison of the different catalogs will be useful to assess the strengths and weaknesses of different cluster search methods, and may lead to a better understanding of the selection effects present in this optically-selected sample.

Since the image mosaic adopted by the EIS provides two sets of frames that contiguously cover the patch, these can be used to extract two independent galaxy catalogs and to generate two independent catalogs of candidate clusters. The comparison between these catalogs is used to quantify the reliability of the cluster detection procedure directly from the data, while simulations based on the extracted galaxy catalogs are used to determine conservative selection criteria that minimize the inclusion of spurious detections in the cluster candidate list presented.

In Sects. 2 and 3 the observations, data reduction and the object catalogs, that are used for the cluster search, are briefly discussed. The cluster finding procedure, based on the matched-filter algorithm proposed by P96, is described in Sect. 4. In Sect. 5 the properties of the detected candidates are discussed. In Sect. 6 conclusions of this work are summarized, and its possible extensions to the search for clusters using the coadded EIS images discussed.

2. Observations and data reduction

The observations for the EIS are being conducted using the EMMI camera (D'Odorico 1990) on the ESO 3.5m New Technology Telescope. The effective field-of-view of the camera is about $9' \times 8.5'$, with a pixel size of 0.266 arcsec. Observations are being carried out over four pre-selected patches of the sky, spanning a wide range in right ascension. In this paper only the data obtained in the first of these patches, at $\alpha \sim 22^h45^m$ and $\delta \sim -40^\circ$ (hereafter Patch A) are used. Observations in this patch were obtained during six different runs, from July to November 1997, and cover a total area of 3.2 square degrees in I band. The I filter that is being used has a wide wavelength coverage, and the response function can be found in Paper I. The EIS magnitude system is defined to correspond to the Johnson-Cousins system, for zero-color stars.

The EIS observations consist of a sequence of 150 sec exposures. Each point of a patch is imaged twice (except at the edges of the patch), for a total integration time of 300 sec, using two frames shifted by half an EMMI-frame both in right ascension and declination. The easiest way of visualizing the global geometry of this mosaic of frames is to consider two independent sets of them, forming contiguous grids (in the following referred to as odd and even frames), superposed and shifted by half a frame both in right ascension and declination.

Observations were carried out in regular visitor mode, and observing conditions varied quite significantly from run to run, and also from night to night within a single run. This fact translates into a considerable spread in the data-quality of different EIS frames. The seeing and limiting 1σ isophote in one arcsec^2 distributions for Patch A observations are shown in Fig. 1 for the odd and even frames. The median values for the combined sample are 1.10 arcsec and 25.42 mag/arcsec^2, respectively. As can be seen both distributions are broad with the seeing reaching 2 arcsec and limiting isophotes 1 mag brighter than the median. Also note that there are small differences in the limiting isophote distributions for the odd and the even frames, which lead to a variation in the depth of the galaxy catalogs as function of position and impact the cluster detection.

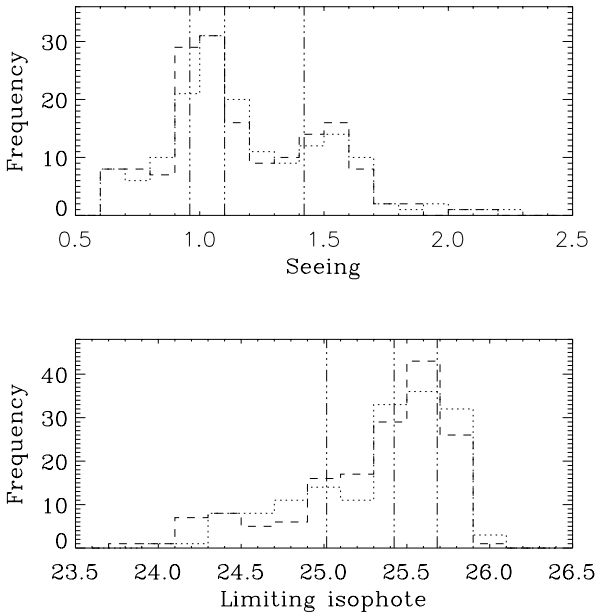

Fig. 1. The data-quality as measured from the seeing and limiting isophote distributions. The top panel shows the seeing distributions for the odd (dashed line) and even (dotted line) tiles in Patch A. The vertical lines mark the 25, 50 and 75 percentiles of the distributions. The median for the combined sample is 1.10 arcsec. The bottom panel shows the distributions of limiting isophotes in mag/arcsec^2. The median limiting isophote for the combined sample is 25.42 mag/arcsec^2.

The data reduction is carried out automatically through the EIS pipeline, described in Paper I. Even though the pipeline was designed to produce coadded images, it also produces fully corrected single frames, using the astrometric and photometric solution derived from the global data reduction process. The astrometric solution is found relative to the USNO-A1 catalog. The internal accuracy of the astrometric solution is better than 0.03 arcsec, although the absolute calibration suffers from the random and systematic errors of the reference catalog. It is important to emphasize, however, that the internal accuracy is more than adequate for the relative positioning of the slits in the first generation of VLT instruments such as FORS. It is also worth reminding that the pointing accuracy of the VLT is foreseen to be no better than 1 arcsec at first light. The photometric calibration is done in a two step procedure first bringing all the frames to a common photometric zero-point, taking advantage of the overlap between the frames, then making an absolute calibration based on external data. The internal accuracy of the photometric calibration is $\lesssim 0.005$ mag. The current absolute calibration uncertainty is $\lesssim 0.05$ mag. Further details can be found in Paper I.

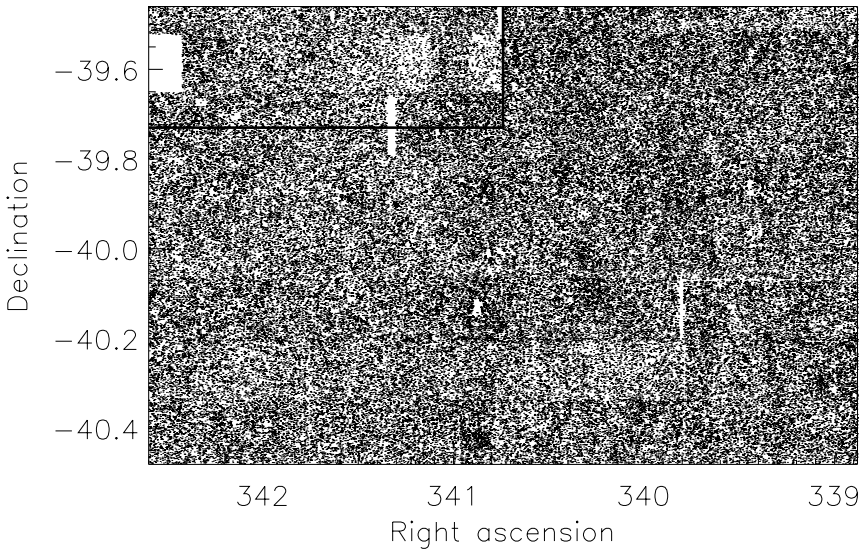

Fig. 2. The projected distribution of galaxies with $I \leq 23$ included in the even I-band catalog for Patch A, limited to the region fully covered by both even and odd tiles. The marked region is the region which was excluded from the analysis because of its obvious incompleteness.

3. Galaxy catalog

In this paper object catalogs extracted from single frames by the EIS reduction pipeline are used. One of the intermediate products of the pipeline is a multiple entry object catalog that includes all detected objects in all individual frames. This object catalog is a multi-purpose element of the pipeline from which several catalogs are derived. Among them are the odd and even catalogs, which are single entry catalogs listing all objects detected in the even or odd frames. To build these catalogs, multiple detections in the small overlap regions are appropriately associated to a single object, as described in Paper I.

Fig. 2 shows the projected distribution of galaxies with $I \leq 23$ from the even catalog of Patch A, for a total of 132,008 objects. The figure only shows the area with full coverage from both even and odd tiles, totaling 2.91 square degrees.

In Paper I the reliability and completeness of the single-frame catalogs were explored by comparing the deep reference field (see Paper I) with the individual frames obtained for that field. Based on that analysis, it was estimated that the single-frame odd and even catalogs are 80% complete to $I = 23.0$ for a typical frame. At that same limiting magnitude the contamination from spurious objects is estimated to be approximately 20%. As shown in Fig. 23 of Paper I, varying observing conditions had a small impact on the object number counts for magnitudes $I \lesssim 23$.

The object classification was shown to be reliable to $I \approx 21$. Brighter than this magnitude all objects with a SExtractor stellarity index < 0.75 are taken to be galaxies, while all detected objects fainter than $I = 21$ are taken to be galaxies. Already at this magnitude the fraction of stars is found to be $\sim$25% of the total number of objects, and taking into account the steep rise of the galaxy number counts faintward of $I = 21$, the contamination of the galaxy catalogs by stars can be considered negligible. Taking into account all objects brighter than the limit for the star/galaxy separation, it is found that the number of objects having different classification in the even and odd catalogs is $\sim$5%.

4. Cluster catalog construction

4.1. Algorithm

Several algorithms are available for an objective search of distant clusters of galaxies, ranging from counts-in-cells (e.g., Lidman & Peterson 1996), to matched filters (e.g. P96; Kawasaki et al. 1997), and surface brightness fluctuations (e.g., Dalcanton 1996). However, the main concern in this preliminary investigation is neither to discuss the relative merits of different algorithms nor to investigate the optimal way of detecting clusters. Instead, the main focus is to investigate the reliability of the detections from a survey conducted under varying observing conditions. This is done by comparing the candidates derived from the two sets of frames available, and also by comparing the surface density and estimated redshift distribution with those derived from the Palomar Distant Cluster Survey (PDCS; P96). From the galaxy number counts presented in Paper I, it was established that the EIS data are of comparable depth to those of P96. Therefore, the first EIS cluster catalogs were constructed using the matched filter algorithm as presented in P96 to facilitate comparisons between the two cluster samples.

Because an extensive description of the algorithm is given by P96, only a brief summary of that discussion is presented here. The matched filter algorithm is designed to filter a galaxy catalog and suppress preferentially those fluctuations in the galaxy distribution that are not due to real clusters. Its most attractive features are: 1) it is optimal for identifying weak signals in a noise-dominated background; 2) photometric information is incorporated along with positional information; 3) the contrast of overdensities that approximate the filter shape is greatly enhanced; 4) redshift and richness estimates for the cluster candidates are produced as a byproduct. The main negative feature of such an algorithm is that one must assume a form for the cluster luminosity function and radial profile. Therefore, clusters with the same richness, but different intrinsic shape, or different luminosity function, do not have the same likelihood of being detected. The filter is derived from an approximate maximum

likelihood estimator, obtained from a model of the spatial and luminosity distribution of galaxies within a cluster. The distribution is represented as

$$D(r,m) = b(m) + \Lambda_{cl} P(r/r_c)\phi(m-m^*) \quad (1)$$

where: $D(r,m)$ is the total number of galaxies per magnitude and per arcsec^2 at a given magnitude m and at a given distance r from the cluster center; $b(m)$ is the background (field galaxy) number counts at magnitude m; $P(r/r_c)$ is the cluster projected radial profile; $\phi(m-m^*)$ is the cluster luminosity function; and Λ_{cl} measures the cluster richness. The parameters m^* and r_c are the apparent magnitude corresponding to the characteristic luminosity of the cluster galaxies and the projected value of the cluster characteristic scale length (core radius), respectively. From this model one can write an approximate likelihood $\mathcal{L}$ of having a cluster at a given position as

$$\ln \mathcal{L} \sim \int P(r/r_c) \frac{\phi(m-m^*)}{b(m)} D(r,m)\, d^2r\, dm \quad (2)$$

The matched filter algorithm is obtained using a series of δ functions to represent the discrete distribution of galaxies in a given catalog, instead of the continuous function $D(r,m)$. The application of the filter to an input galaxy catalog is therefore accomplished by evaluating the sum

$$S(i,j) = \sum_{k=1}^{N_g} P(r_k) L(m_k) \quad (3)$$

where $P(r_k)$ is the angular weighting function (radial filter), and $L(m_k)$ is the luminosity weighting function (flux filter), at every point (i,j) in the survey, and over a range of redshifts (which corresponds to a range of r_c and m^* values).

In practice, since the optimal flux filter $L(m_k) = \phi(m_k - m^*)/b(m_k)$ has a divergent integral at the faint magnitude limit when ϕ is a Schechter function (Schechter 1976), it is necessary to modify this filter. The solution proposed by P96 is to introduce a power-law cutoff of the form $10^{-\beta(m-m^*)}$ that, with $\beta = 0.4$, would correspond to an extra weighting by the flux of the galaxy. The optimal radial filter is given by the assumed cluster projected radial profile. Here a modified Hubble profile is used, truncated at an arbitrary radius which is large compared to the cluster core radius. Therefore the flux and radial filter have the form

$$L(m) = \frac{\phi(m-m^*)10^{-\beta(m-m^*)}}{b(m)} \quad (4)$$

and

$$P(r/r_c) = \frac{1}{\sqrt{1+(r/r_c)^2}} - \frac{1}{\sqrt{1+(r_{co}/r_c)^2}} \quad (5)$$

where $\phi(m-m*)$ is taken to be a Schechter function, r_c is the value of the projected cluster core radius, and r_{co} is the arbitrary cutoff radius. One further correction to the algorithm is required. The normalization adopted for the flux filter is made according to Eq. (21) in P96. This normalization is in fact only strictly correct for a pure background distribution, but introduces an error in the redshift estimate of cluster candidates when an overdensity of galaxies is present. To compensate for this effect, and obtain a corrected filter $S_{corr}(i,j)$, the same procedure proposed by P96 (their Eqs. 22–26) was adopted here.

4.2. Cluster-finding pipeline

The matched filter algorithm described above is the central component of the EIS cluster searching pipeline that was implemented to process the galaxy catalogs produced by the EIS reduction pipeline. In this section the details about its implementation, and the methods adopted to identify significant cluster candidates are described.

Because of the large size of the patches, they are divided into overlapping sub-areas, to avoid edge effects in the final candidate catalog. The size of the sub-regions are typically 1 square degree, but are chosen to match the geometry of the region, after bad areas are removed. This procedure also allows the cluster-finding to use a more local background.

The matched-filter is applied to each of the sub-catalogs by evaluating the sum $S_{corr}(i,j)$ for each element of a two-dimensional array (i,j), to create a filtered image (hereafter the "Likelihood map") of the galaxy catalog. The elements (i,j) correspond to a series of equally spaced points that cover the entire survey area. At each point (i,j) the sum is evaluated a number of times, with the radial and flux filters tuned to different cluster redshift values in steps Δz =0.1 (this will hereafter be called the "filter redshift"). The minimum adopted filter redshift is $z_{min} = 0.2$, while the maximum redshift z_{max} is determined by finding the redshift value at which the apparent characteristic magnitude $m^*(z)$ becomes comparable to the limiting magnitude of the catalog. This approach gives a $z_{max} = 1.3$ for the typical limiting magnitude of $I = 23$. The characteristic luminosity M^* and the cluster core radius are assumed to remain fixed in physical units, and also the luminosity function faint-end slope, α, is fixed. The observable quantities m^* and r_c are assumed to vary with redshift as in an H_0=75 km s^{-1}/Mpc , Ω_0=1 standard cosmology. The adopted cluster parameters, taken from P96, are $r_c = 100h^{-1}$kpc, $r_{co} = 1h^{-1}$Mpc and $M_I^* = -22.33$. The value of M_I^* was corrected to the Cousins system adopting the transformation given in P96.

Both a non-evolving galaxy model, and a model with passive evolution of the stellar population have been considered. In this paper only the results obtained using a non-evolving model, based on a template spectrum of an elliptical galaxy taken from Coleman et al. (1980) are presented. It is important to emphasize that the choice of the K-correction model does not significantly impact the cluster detections.

The pixel size of the Likelihood maps (i.e. the spacing between adjacent (i,j) array elements) is taken to be 26.3 arcsec, corresponding to the value of the projected cluster core radius, for a cluster at a redshift of 0.6. Ideally, one would like to have a varying pixel size, corresponding to a fixed fraction of a cluster projected core radius at all filter redshifts. However, this would complicate the comparison between Likelihood maps obtained with different filter redshift, and since this comparison is ex-

tremely useful for distinguishing real peaks from noise fluctuations (see Sect. 4.3), it was decided to use a fixed pixel size for the creation of the maps.

Given the typical redshift limits discussed above, 12 Likelihood maps are created from each input galaxy catalog, and these are stored as FITS-images, for ease of manipulation. Significant peaks in the likelihood distribution are identified independently in each map, using SExtractor. The mean and variance of the background are determined using a global value in each Likelihood map and peaks with more than N_{min} pixels with values above the detection threshold σ_{det} are considered as potential detections. At each filter redshift, the value of N_{min} is set to correspond to the area of a circle with radius $\sim 1 r_c$, while the value of σ_{det} is kept constant at 2. These parameters were optimized using the simulations described in Sect. 4.3. The significance of a detection is obtained comparing the maximum value of the signal among the pixels where the likelihood is above the SExtractor detection threshold with the background noise.

The lists of peaks identified in the various Likelihood maps are then compared and peaks detected at more than one filter redshift are associated on the basis of positional coincidence. From this association, likelihood versus z curves are created, and those peaks that persist for at least four filter redshifts (see Sect. 4.3) are considered as *bona fide* cluster candidates. The redshift and richness estimates for each candidate are derived locating the peak of the corresponding likelihood versus z curve. The significance of a candidate detection is measured as the maximum of the significance versus z curves, regardless of the estimated redshift of the candidate cluster.

Two richness parameters are derived, following P96. The first is obtained from the matched filter procedure itself, using the parameter Λ_{cl} introduced in Eq. (1). This parameter is computed using Eq. (29) in P96, and the Likelihood map corresponding to the cluster estimated redshift. A second independent richness estimate, N_R, is defined to allow for a comparison with the conventional Abell richness parameter. It is the number of member galaxies (i.e. the number of galaxies above the estimated background) within a two-magnitudes interval delimited on the bright side by the magnitude of the third brightest cluster member. This galaxy is identified within a circle of radius $0.25h^{-1}$ Mpc, centered on the nominal position of the cluster detection. The magnitude distribution for all galaxies within this circle is derived using 0.20 mag bins, and the expected background contribution is subtracted from it. The background magnitude distribution is determined using the entire galaxy catalog and the same magnitude bins. Note that this procedure makes this parameter very sensitive to variations in the background, leading to large uncertainties, especially for the more distant candidates. Within this background-subtracted magnitude distribution the bin that contains the third brightest galaxy is identified. The entire procedure is then repeated for a circle of radius $1.0h^{-1}$ Mpc, keeping m_3, the magnitude of the third brightest galaxy, fixed to the value determined within the smaller $0.25h^{-1}$ Mpc radius circle. To reduce the probability that a foreground field galaxy on the line of sight to the cluster could bias the richness estimate, the third brightest galaxy is constrained to be fainter than $m^* - 3$, where m^* is computed for the cluster estimated redshift.

The final step in producing the cluster candidate catalogs is the cross-matching between the even and odd detections. The pairing is done based on positional coincidence only, and the maximum distance between the two nominal centers must be less than 1 arcmin, which corresponds roughly to two Likelihood map pixels. The allowed separation was determined from the estimated uncertainty in the position measurements. The latter was estimated by comparing the position of the nominal centers for typical even/odd detections.

4.3. Tests of the algorithm

Simulated galaxy catalogs were used to establish the best choice of extraction parameters used in the pipeline, namely those that minimize the frequency of noise peaks. Two areas of patch A, covering an area of 0.6 square degrees each, were selected to represent a uniform (in terms of seeing and limiting isophote) and a typical (i.e. non-uniform) region of the entire surveyed area. Using both the even and the odd catalogs there are 4 catalogs available to cover these two areas. From each of these catalogs 25 background-only simulated galaxy catalogs were created by randomly repositioning the galaxies (within the same area), while keeping their magnitudes fixed. This procedure neglects the small correlation that is present between galaxy projected positions on the sky, but the amplitude of the galaxy-galaxy angular two-point correlation function is small enough at the magnitudes of interest here, that this approximation should have negligible impact on the simulation results.

Using these simulated catalogs it was possible to quantify the noise-rejection capabilities of the cluster finding procedure. The results obtained with the four sets of simulations are all equivalent, and are not distinguished in the following discussion. The simulated catalogs were processed through the cluster-finding pipeline, and the peak-identification process was run a number of times, using a range of different settings for the two SExtractor detection parameters: the minimum number of pixels above the detection threshold, N_{min}, and the detection threshold itself, σ_{det}, expressed in units of the Likelihood map variance. It was found that noise peaks are best rejected when N_{min}, at all redshifts, is chosen to be roughly comparable to the area of a circle with radius the assumed cluster core radius. The adaptive N_{min} compensates for the fixed Likelihood maps pixel scale mentioned in the previous section.

In Table 1 the results obtained applying different detection strategies to the background-only simulations are presented. The number of detections that were found in the simulations, scaled to a common reference area of one square degree, are reported as a function of different SExtractor detection thresholds, of the adopted persistency criterion, and of the lack or presence of further restrictive criteria on the richness or the significance associated with the detection. As can be seen, a SExtractor threshold of $\sigma_{det} = 3.0$ gives a good rejection of noise peaks, with at least a factor of 3 fewer spurious detections than the lower thresholds. To investigate the effect of this threshold on the

Table 1. Frequency of expected spurious detections per square degree.

	$\sigma_{det} = 1.5$	$\sigma_{det} = 2.0$	$\sigma_{det} = 3.0$
All	46.3	56.4	13.3
$n_z \geq 4$	27.5	14.3	0.4
$n_z \geq 4, \sigma \geq 3$	14.7	9.0	0.2
$n_z \geq 4, \sigma \geq 4$	3.0	1.7	0.4
$n_z \geq 4, \sigma \geq 3, \Lambda_{cl} \geq 30$	5.1	4.6	0.3
$n_z \geq 4, \sigma \geq 4, \Lambda_{cl} \geq 30$	0.4	0.4	0.2

extracted candidate lists the detection rates from the real and simulated data were compared. This showed that applying a threshold of $\sigma_{det} \geq 3.0$ decreased the number of detections in the real and simulated data by similar amounts, while lower thresholds preferentially rejected spurious peaks in the simulated data. Therefore, a $\sigma_{det} = 3.0$ threshold was considered to be too restrictive. On the other hand, because the automatic SExtractor de-blending procedure can override the specified N_{min} criterion, it was decided not to use it and therefore a low threshold of $\sigma_{det} = 1.5$ resulted in too many blended peaks. As a compromise a detection threshold of $\sigma_{det} = 2.0$ was adopted.

This threshold results in many spurious detections and therefore other properties of the noise generated peaks were used to minimize their contribution. Fig. 3 shows the distribution of the most relevant of these properties as derived using the SExtractor parameters N_{min} corresponding to the number of pixels contained within a circle of radius $1r_c$ and $\sigma_{det} = 2.0$. The frequency of detected peaks (scaled to a one square degree projected area) is plotted as a function of the detection significance, of the number of filter redshifts, n_z, where the detection took place, and of the inferred cluster richness, Λ_{cl}. From the figure it can be seen that in addition to the detection significance, the number of filter redshifts at which the peak appears is a valuable tool for discriminating noise peaks. Typically, noise peaks appear in only a few redshift shells, while clusters are detected in more than five. Therefore, candidate clusters are required to be detected in at least four redshift shells. The lower panel of Fig. 3 shows another useful noise discriminant, namely the inferred richness, Λ_{cl}, which for the noise peaks is rarely above Λ_{cl} =30. Therefore the requirement that the inferred richness should be $\Lambda_{cl} \geq 30$ has been used as a third criterion for the cluster candidate selection.

From Table 1 the effect of the different noise rejection criteria can be seen. For the selected detection parameters of the adaptive N_{min}, discussed above, and $\sigma_{det} = 2.0$, the additional criteria of the number of filter redshifts $n_z \geq 4$ and inferred richness $\Lambda_{cl} \geq 30$ were adopted. These criteria yield a frequency of noise peaks ~ 0.4 per square degree in the case of a restrictive significance $\geq 4\sigma$, and ~ 4.6 if a significance ≥ 3 is adopted. For comparison, the expected frequency of spurious detections in the PDCS is 0.8 per square degree when peaks with significance $\geq 4\sigma$ are considered, and 4.2 per square degree when peaks with significance $\geq 3\sigma$ are taken into account.

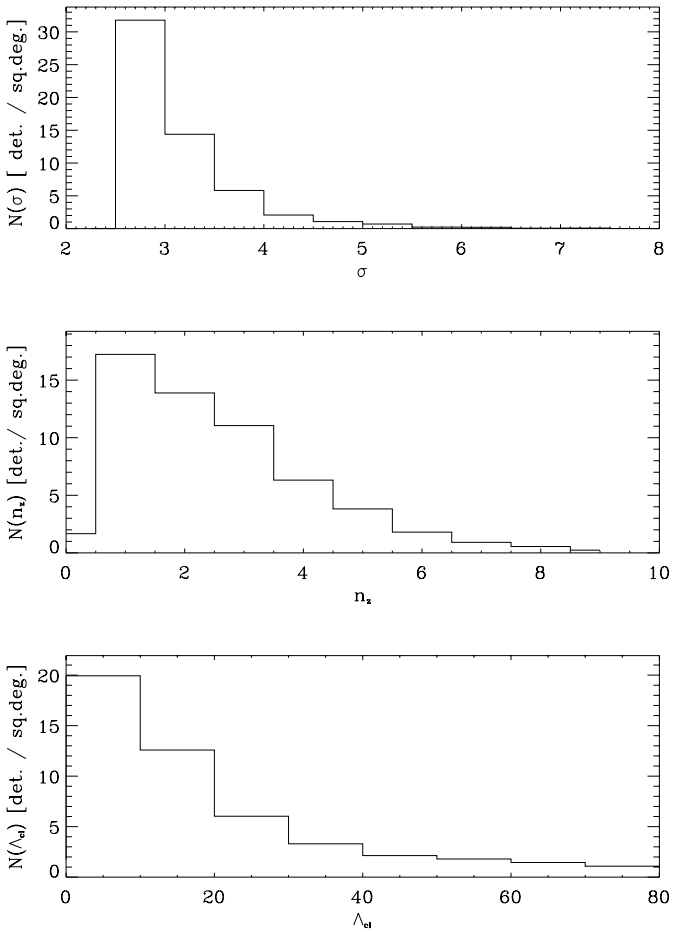

Fig. 3. The properties of noise-generated peaks in the background-only simulations. The three panels show the frequency distribution (scaled to a one square degree projected area) of noise peaks as a function of the detection significance, of the number of filter redshifts where the detection took place, and of the inferred richness. The SExtractor detection parameters used here is N_{min} corresponding to a circle of $1r_c$ and $\sigma_{det} = 2$.

5. Results

The cluster-finding procedure described in the previous section was applied to Patch A even and odd single-frame catalogs. To facilitate a comparison between the derived cluster candidates, the search was restricted to the region of overlap between the odd/even galaxy catalogs. Furthermore, a region at the north-east corner of the patch was discarded, because of severe incompleteness. The effective area searched is delineated in Fig. 2, covering 2.5 square degrees.

Using the cluster model described in Sect. 4.2 and the selection criteria described in the previous section, the cluster catalog presented in Table 2 was constructed. The upper part of the table lists the "good" candidates, which are those with significance $\geq 4\sigma$, in at least one catalog or with a significance $\geq 3\sigma$ in both catalogs, while the lower part gives the candidates detected at 3σ in only one catalog. In both cases the additional criteria of detection requiring $n_z \geq 4$ and $\Lambda_{cl} \geq 30$ are imposed. Furthermore, all candidates with significance $\geq 5\sigma$ and $n_z \geq 4$,

Table 2. Preliminary EIS cluster catalog

Cluster name	α (J2000)	δ (J2000)	z_{noevol}	Λ_{cl}	N_R	σ_{even}	σ_{odd}	Notes
EIS 2236−3935	22 36 02.9	−39 35 33.7	0.3	44.5	12	4.9	4.9	
EIS 2236−4017	22 36 18.0	−40 17 54.9	0.6	107.8	47	5.8	6.8	
EIS 2236−4026	22 36 47.6	−40 26 17.4	0.4	44.0	15	–	4.2	
EIS 2237−4000	22 37 11.4	−40 00 16.1	0.3	31.3	30	3.8	4.6	
EIS 2237−3932	22 37 45.3	−39 32 11.8	0.2	30.1	42	4.1	4.1	EDCC 169
EIS 2238−3934	22 38 03.4	−39 34 50.4	0.3	41.8	40	4.4	–	
EIS 2238−3953	22 38 46.4	−39 53 41.9	0.6	57.5	36	3.3	3.0	
EIS 2239−3957	22 39 17.3	−39 57 03.3	0.5	56.1	40	–	4.0	
EIS 2239−3954	22 39 18.4	−39 54 34.9	0.3	62.5	25	6.2	6.8	
EIS 2240−4021	22 40 07.8	−40 21 08.0	0.3	41.2	21	4.9	5.4	
EIS 2241−4001	22 41 19.0	−40 01 15.9	0.9	232.2	87	3.5	5.2	
EIS 2241−4006	22 41 26.7	−40 06 24.7	0.3	32.6	22	4.9	3.9	
EIS 2241−3932	22 41 31.3	−39 32 10.4	0.4	44.5	14	4.0	4.2	
EIS 2241−3949	22 41 42.1	−39 49 14.6	0.2	47.9	30	7.1	8.1	
EIS 2243−4013	22 43 01.3	−40 13 58.2	0.2	36.3	16	6.1	5.9	
EIS 2243−4010	22 43 01.9	−40 10 24.8	0.3	39.1	26	5.4	–	
EIS 2243−3952	22 43 19.4	−39 52 41.2	0.3	50.9	27	6.2	–	S1055
EIS 2243−4025	22 43 23.8	−40 25 49.9	0.2	28.9	6	6.2	5.5	
EIS 2243−3959	22 43 29.4	−39 59 33.5	0.3	45.0	32	4.5	5.5	
EIS 2243−4008	22 43 47.4	−40 08 47.0	0.3	34.3	30	–	4.4	*
EIS 2243−3947	22 43 56.1	−39 47 28.8	0.4	48.6	34	4.1	–	
EIS 2244−4014	22 44 01.0	−40 14 29.6	0.6	75.7	33	–	4.2	
EIS 2244−3955	22 44 23.2	−39 55 23.6	0.2	41.7	20	5.6	–	*
EIS 2244−4019	22 44 28.4	−40 19 46.5	0.3	38.3	27	4.9	4.6	
EIS 2246−4012	22 46 30.1	−40 12 48.4	0.2	34.6	19	5.8	–	
EIS 2246−4012	22 46 48.5	−40 12 48.2	0.4	39.5	32	3.2	3.6	
EIS 2248−3951	22 48 28.7	−39 51 24.6	0.5	49.4	15	3.4	3.4	*
EIS 2248−4015	22 48 54.8	−40 15 18.8	0.3	36.2	26	4.6	4.4	
EIS 2249−4016	22 49 33.9	−40 16 33.7	0.6	63.2	42	3.4	3.6	
EIS 2236−4008	22 36 46.0	−40 08 45.2	1.0	184.1	49	3.1	–	*
EIS 2238−4001	22 38 33.8	−40 01 50.9	0.7	97.0	24	3.9	–	*
EIS 2238−4010	22 38 36.0	−40 10 36.6	0.8	89.1	20	3.0	–	*
EIS 2239−3946	22 39 34.4	−39 46 41.8	0.7	67.9	82	3.1	–	
EIS 2244−4013	22 44 59.3	−40 13 08.1	0.9	130.2	82	2.6	3.2	*
EIS 2249−3958	22 49 33.0	−39 58 10.1	0.9	123.6	29	–	3.1	

regardless of their richness, were included. The results show that there are 26 "good" detections in the even and 23 in the odd catalog. As discussed below, most of these represent paired detections. For lower significances, one finds 5 detections in the even and 2 in the odd catalog, respectively.

For each cluster, Table 2 gives: in column (1) the cluster ID; columns (2) and (3) the J2000 equatorial coordinates; in column (4) the estimated redshift using a K-correction obtained assuming no evolution of the stellar population; in columns (5) and (6) the richness estimates Λ_{cl} and N_R; in columns (7) and (8) the significance for the detection in the even and odd catalog, if available; and in column (9) an asterisk indicates doubtful cases based on the visual inspection of the coadded image. When a candidate cluster is detected in both the even and odd catalogs, the redshift and richness estimates presented in the tables are the ones derived from the catalog where the highest likelihood value was measured. In total 29 "good" candidates are reported, giving a density of 11.6 per square degree.

Of the 26 "good" detections found in the even catalog 19 (73%) have a counterpart in the odd, while for the 23 detections in the odd catalog 19 (83%) have a counterpart in the even. For the sample as a whole the probability of having a counterpart in the other catalog is still reasonably high −65% for detections in the even catalog and 80% for the odd. The observed difference in the frequency of paired detections between the two catalogs is probably due to variations in the observing conditions. Overall the even frames tend to have fainter limiting isophotes than the odd (Fig. 1) which may explain the larger number of detections in the even catalog. Furthermore, inspection of the limiting isophote maps shows, that in general, objects of high significance in one catalog not detected in the other lie in regions where significant variations of the limiting isophotes are seen. Therefore, the results reflect the lack of homogeneity of the data.

In Fig. 4 the projected distribution of the detected cluster candidates is shown. There is a clear paucity of clusters in the

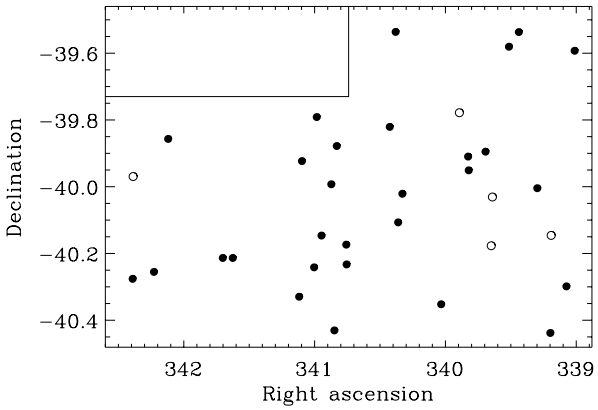

Fig. 4. The projected distribution of the cluster candidates. The filled circles are the "good" candidates, while the open circles represent the 3σ candidates detected in only one catalog.

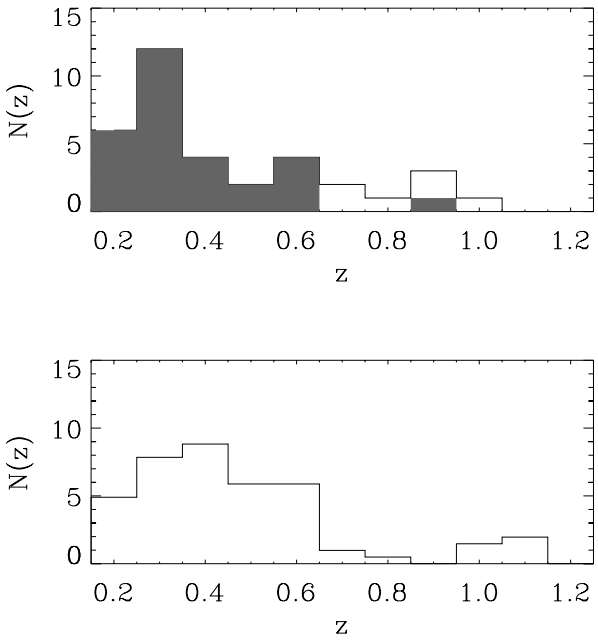

Fig. 5. The upper panel shows the redshift distribution of the cluster candidates in Table 2. The shaded area is the distribution of the good clusters while the white area shows the additional contribution from the less robust candidates. The lower panel shows the redshift distribution for the cluster candidates from the PDCS scaled to an area of 2.5 square degree for comparison.

region around the position $\alpha \sim 341.5°$ and $\delta \sim -40.0°$. Inspection of the seeing and limiting isophote maps shows that the data in that region are reasonably uniform and deep, and the lack of clusters in the region is probably real. In the region considered in the present paper there are four clusters listed in NED. Out of these two have also been identified in the present work. These are S1055, which is located behind the bright galaxy ESO 345-G046, and EDCC 169. Those not identified are EDCC 163 and a Lidman & Peterson (1996) cluster (Cl2245-4002), both of which lie at the edges of the region considered in this paper.

For each cluster cutouts from the coadded image are created, covering a region of 7×7 arcmin centered at the nominal position of the detection. The area covered roughly corresponds to the FORS field of view. These cutouts are available at "http://www.eso.org/eis/". Also available are image postage stamps from all the passbands available at a given cluster position. Using these postage stamps all cluster candidates were visually inspected. As a result, a note was added to Table 2, to indicate doubtful cases. Note that most of these are in fact found in the lower part of the table, associated with lower significance detections. Of the "good" candidates only three are doubtful, all at the edges of overlapping frames (in the language of the coadded image presented in Paper I, near the border of different contexts). It is also worth pointing out that 11 out of the 16 candidates not detected in both even and odd frames are located near the border of regions where the quality of the images vary significantly. Most of these cases are located near the shallower region centered at $\delta \sim -40°12'$ ($\delta \sim -40.2°$) clearly visible in Fig. 2. However, it should be noted that the eye-balling did not indicate that these candidates are less promising than in other regions. Another example is the candidate EIS 2243−4008 found near the brightest star in the region. This shows that the cluster finding method as currently implemented is not optimized for dealing with inhomogeneous data of the sort presented here. since it implicitly assumes a fairly homogeneous background.

In Fig. 5 the redshift distribution of the total candidate sample is shown and compared to the distribution for the candidates reported in the PDCS. Considering the small number of candidates, the redshift distribution of EIS candidate clusters agrees well with that determined for PDCS. The shaded area represents the redshift distribution of the "good" candidates. The distribution of these candidates covers the redshift range from 0.2 to 0.9, while the total sample extends to $z = 1$ with a median redshift of $z = 0.3$.

Fig. 6 shows the distributions of the two cluster richness estimates, comparing those for the total cluster sample with the "good" candidates. As can be seen the Λ_{cl} richness spans a wide range extending up to ~ 230 with a median of ~ 45.0. The Abell richness estimate, N_R, is found to vary between 6 and 87 with a median of 29. Note that in the case of richness an appropriate comparison with the results of P96 cannot be made because of our imposed richness criterion in the detection and differences between the estimates of the mean background counts in the calculation of the Abell richness in this paper and in P96.

A comparison between the estimates of the candidates' properties, discussed in the previous section, is used to obtain a rough estimate of their accuracy. Fig. 7 shows a comparison of the estimated redshifts for all paired detections, as determined in the odd/even catalogs. Some of the points represent more than one cluster candidate due to the discreteness of the redshift bins. The mean difference of the two redshift estimates is found to be small ~ 0.01. Similarly, Fig. 8 shows the comparison of the Λ_{cl} richness estimates. As can be seen, in general they agree remarkably well. The average difference in the estimates relative to their mean value is about 10%. There is only one large disagreement found for a candidate cluster at $z \sim 0.9$ with very

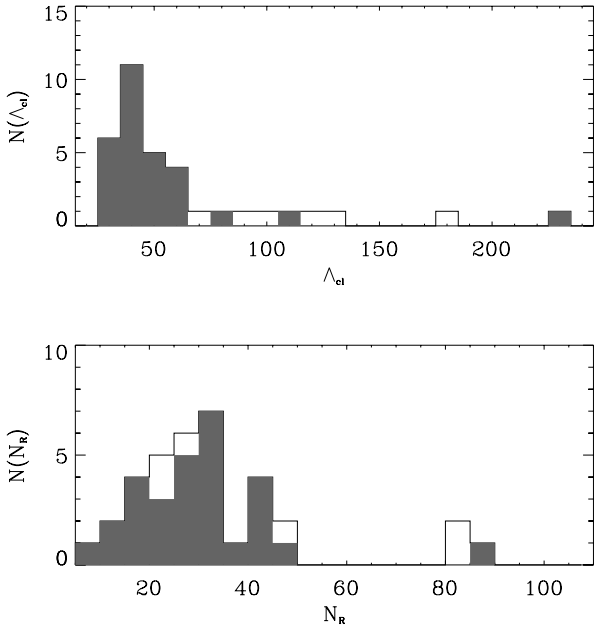

Fig. 6. The upper panel shows the distribution of the richness measure Λ_{cl}, the shaded area is the distribution of the good candidates and the white shows the additional contributions from the less robust candidates. The lower panel shows the distribution of Abell richness.

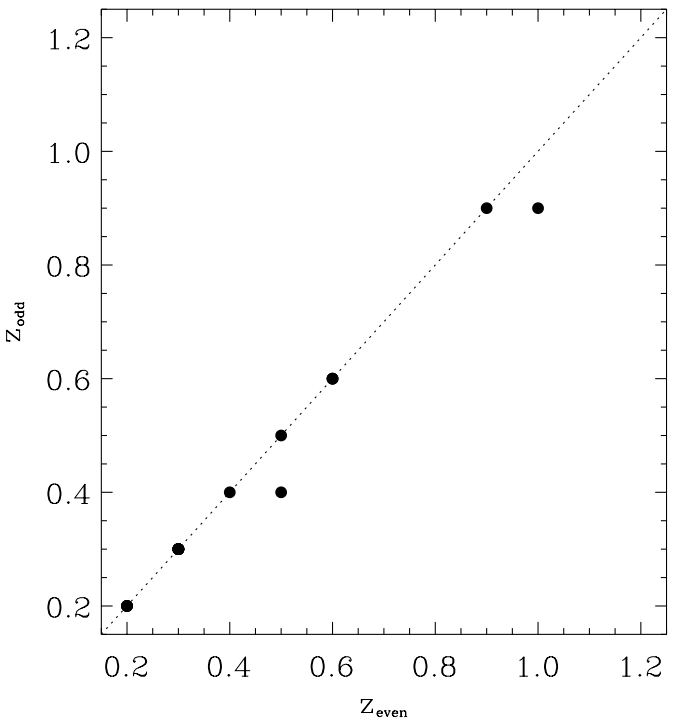

Fig. 7. Comparison of the matched filter redshifts derived from the even and odd catalogs. Most points along the diagonal (dotted line) represent more than one detection due to the redshift grid.

different significances in the two catalogs, thus leading to different richness estimates. Note that this candidate also corresponds to one of the deviant points in the redshift comparison.

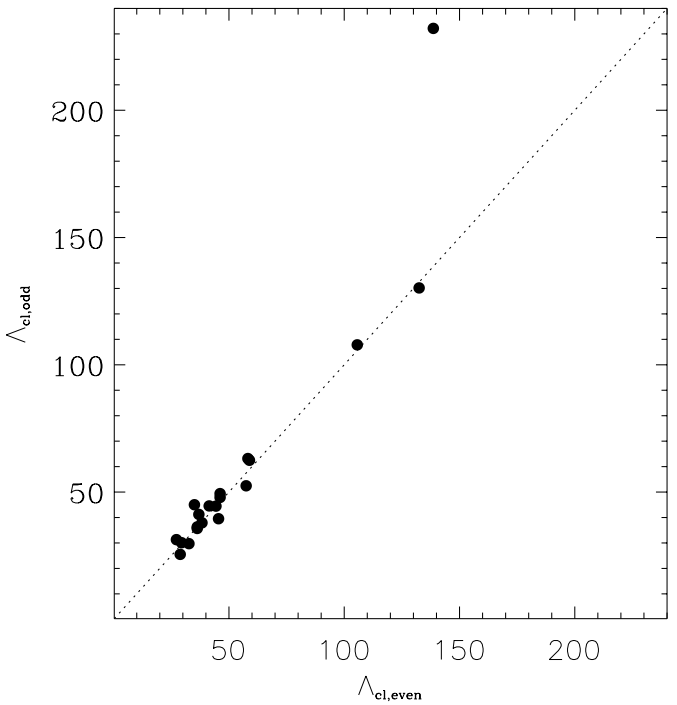

Fig. 8. Comparison of the Λ_{cl} richness estimates as derived from the even and odd catalogs. The dotted line represents the slope equal one line.

6. Summary and future developments

The recently released EIS I-band data for Patch A ($\alpha \sim 22^h45^m$ and $\delta \sim -40°$; see Paper I) have been used to search for clusters of galaxies over an area of 2.5 square degrees, in the redshift range $0.2 \leq z \leq 1.3$. The matched filter algorithm has been applied to the even and odd single-frame catalogs to assess the performance of the cluster-finding pipeline, to establish the detection threshold for robust detections and to evaluate the quality of the EIS data for this kind of analysis, one of the main goals of the survey.

The candidate cluster sample of "good" detections consists of 29 objects, yielding a surface density of 11.6 candidates per square degree, with a median redshift of $z = 0.3$. When all 3σ detections are considered 35 candidates are found, leading to a surface density of 14 per square degree. Both the redshift distribution and the surface density of candidates are consistent with the results of P96. To help users to evaluate these candidates and to prepare finding charts, image postage stamps are available at "http://www.eso.org/eis/".

These results should be considered preliminary as significantly better data are available for the other EIS patches. More importantly, the use of catalogs extracted from the coadded images will allow a deeper cluster search to be carried out, thereby extending the redshift range for the cluster sample. Clearly, the EIS data more than fulfills the science requirements of the survey, as originally stated.

In this first release of the EIS cluster catalog the effort has been concentrated on the I-band data. However, a limited number of frames in V-band have been obtained and will be used

to further investigate the candidate clusters over the surveyed region (Olsen et al. 1999).

Acknowledgements. The data presented here were taken at the New Technology Telescope at the La Silla Observatory under the program IDs 59.A-9005(A) and 60.A-9005(A). We thank all the people directly or indirectly involved in the ESO Imaging Survey effort. In particular, all the members of the EIS Working Group for the innumerable suggestions and constructive criticisms, the ESO Archive Group for their support and for making available the computer facilities, ST-ECF for allowing some members of its staff to contribute to this enterprise. To the Directors of Copenhagen, IAP, Institute of Radio Astronomy in Bologna, Heidelberg, Leiden, MPA, Trieste and Turin for allowing the participation of their staff in this project and for suggesting some of their students and post-docs to apply to the EIS visitor program. Special thanks to G. Miley, who facilitated the participation of ED in the project and for helping us secure observations from the Dutch 0.9m telescope. To the Geneva Observatory, in particular G. Burki, for monitoring the extinction during most of the EIS observations. To the NTT team for their help. This research has made use of the NASA/IPAC Extragalactic Database (NED) which is operated by the Jet Propulsion Laboratory, California Institute of Technology, under contract with the National Aeronautics and Space Administration. We are also grateful to N. Kaiser for the software. Special thanks to A. Baker, D. Clements, S. Coté, E. Huizinga and J. Rönnback, former ESO fellows and visitors for their contribution in the early phases of the EIS project. Our special thanks to the efforts of A. Renzini, VLT Programme Scientist, for his scientific input, support and dedication in making this project a success. Finally, we would like to thank ESO's Director General Riccardo Giacconi for making this effort possible.

References

Coleman G.D., Wu C.-C., Weedman D.W., 1980, ApJS 43, 393
Dalcanton J.J., 1996, ApJ 466, 92
D'Odorico S., 1990, Messenger 61, 51
Kawasaki W., Shimasaku K., Doi M., Okamura S., 1997, astro-ph/9705112
Lidman C.E., Peterson B.A., 1996, AJ 112, 2454
Nonino M., Bertin E., da Costa L., et al., 1999, A&A, in press; astro-ph/9803336 (Paper I)
Olsen L.F., Scodeggio M., da Costa L., et al., 1999, A&A, in press; astro-ph/9807156
Postman M., Lubin L.M., Gunn J.E., et al., 1996, AJ 111, 615 (P96)
Renzini A., da Costa L.N., 1997, Messenger 87, 23
Schechter P., 1976, ApJ 203, 557